

UC Irvine

Faculty Publications

Title

The leaky funnel model revisited

Permalink

<https://escholarship.org/uc/item/57m8g1z9>

Journal

Tellus A, 64(0)

ISSN

1600-0870 0280-6495

Authors

Mouchet, Anne
Deleersnijder, Eric
Primeau, Francois

Publication Date

2012-09-14

DOI

10.3402/tellusa.v64i0.19131

License

[CC BY 4.0](#)

Peer reviewed

The leaky funnel model revisited

By ANNE MOUCHET^{1*}, ERIC DELEERSNIJDER^{2,3} and FRANCOIS PRIMEAU⁴, ¹*Astrophysics, Geophysics and Oceanography Department, Université de Liège, Liège, Belgium;* ²*Institute of Mechanics, Materials and Civil Engineering (iMMC), Université catholique de Louvain, Louvain-la-Neuve, Belgium;* ³*Earth and Life Institute (ELI), Georges Lemaître Centre for Earth and Climate Research (TECLIM), Université catholique de Louvain, Louvain-la-Neuve, Belgium;* ⁴*Department of Earth System Science, University of California at Irvine, Irvine, California, USA*

(Manuscript received 23 May 2011; in final form 29 June 2012)

ABSTRACT

A former publication proposed an idealised view of the global ocean ventilation consisting in a flow through a porous pipe with decreasing section (a leaky funnel). The agreement between the domain-averaged ages as obtained with a coarse-grid 3-D ocean general circulation model (OGCM) and the leaky funnel is excellent. Further, the latter allows to infer characteristic scales, which are consistent with the current knowledge of the ocean ventilation. However, the method, based on numerical experiments in which the circulation fields of the OGCM were artificially modified, is questionable. Here, we revisit the leaky funnel and base our study on the global water age distribution $\varphi(\tau)$, where $\varphi(\tau)\Delta\tau$ is the ocean volume fraction with age in the interval $[\tau, \tau + \Delta\tau]$. The steady-state analytical solution for this distribution is shown to be in excellent agreement with numerical results from two coarse grid OGCMs: an outcome that helps strengthening the leaky funnel representation. The asymptotic analysis of $\varphi(\tau)$ suggests that, for large ages, water parcels have the same life expectancy, whatever their age. Further, the leaky funnel provides bulk characteristics of the circulation in OGCMs, which may serve as metrics in model intercomparison studies.

Keywords: age, distribution function, world ocean, ventilation, model

1. Introduction

The rate at which the ocean can sequester excess heat and carbon from the atmosphere is determined by its ventilation, i.e. the renewal of interior waters by seawater that has been in contact with the atmosphere. In the context of climate and environmental studies, it is of importance to better assess the ocean ventilation rate and its properties. The age, which measures the time needed for water parcels to travel from the ocean surface to the interior, is the appropriate tool for this purpose. Of use are numerical simulations and field measurements of appropriate tracer concentrations. However, the intrinsic complexity of ocean circulation and the huge amount of information provided by ocean general circulation models (OGCMs) make it difficult to extract the most relevant information on spatial and temporal scales characterising ventilation. On the other hand, low-order representations of the world ocean circu-

lation, despite their simplifying hypotheses, very often supply the means allowing one to gain some insight into the main flow characteristics (e.g. Munk, 1966; Craig, 1971; Maier-Reimer, 1993; Jenkins, 1998; Munk and Wunsch, 1998; Broecker and Peng, 2000).

Along this line, Mouchet and Deleersnijder (2008) (hereinafter referred to as MD08) suggested an idealised model, which provides a scaling of the water age. A 1-D advection-diffusion model is proposed in which the interior ocean is represented as a leaky pipe with decreasing section (i.e. a leaky funnel) – allowing recirculation of water and tracers toward the surface (Fig. 1). The analytical solutions to the steady-state problem are readily obtained and yield expressions of the domain-averaged ages as functions of three independent parameters, which determine the flow characteristic scales. A series of experiments with a 3-D OGCM allow for the calibration and assessment of the leaky funnel representation. The agreement between the domain-averaged ages (water and radiocarbon) as obtained with the OGCM and with the leaky funnel is excellent. Moreover, the parameters derived from this exercise have a clear physical meaning; the turnover time, the mean length

*Corresponding author.
email: A.Mouchet@ulg.ac.be

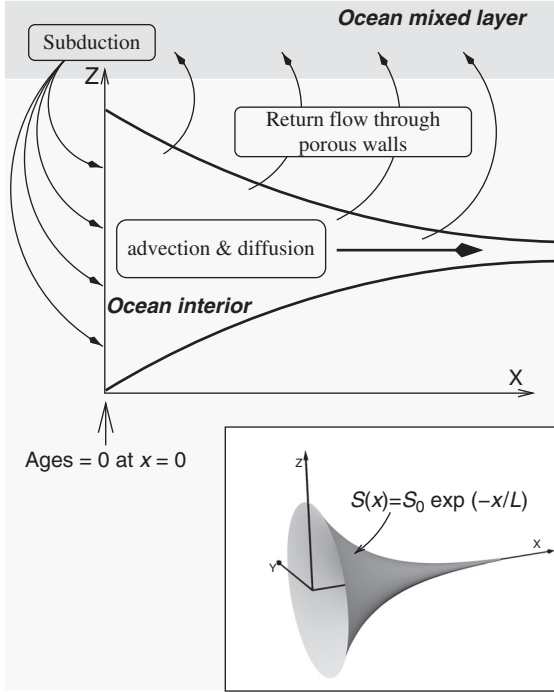


Fig. 1. Schematic representation of the leaky funnel model. A 3-D view is given in the inset while the main figure consists of a projection onto the x - z plane. The leaky funnel extends from $x = 0$ to $x = \infty$ with a decreasing section. The entrance of the funnel is fueled with water from the ocean surface. The porous walls allow water to escape the funnel. Advection and diffusion control the transport within the funnel. At the entrance (boundary at $x = 0$), concentrations are set to unity and ages to zero. It is noteworthy to mention that no assumption is made on the nature of the flow outside the funnel nor on the actual position with respect to the mixed layer.

of trajectories and the diffusivity scale being consistent with our current knowledge of the World Ocean circulation.

Yet, despite these converging results, MD08 raised concerns about the calibration method. Specifically, their method disregards the OGCM internal dynamics. MD08 generated a set of dynamical fields by multiplying by spatially uniform values the reference velocity and diffusivity fields from the OGCM. A similar approach was previously used by Heinze et al. (1991) in the search for the causes of the glacial–interglacial atmospheric CO_2 variations. However, these artificial solutions do not represent possible oceanic circulation states. Indeed, performing experiments in which the diffusivity and the velocity fields are independently multiplied by spatially homogeneous values is in contradiction with the OGCM internal dynamics (buoyancy, momentum, surface forcing, etc.) and satisfy none of the finite-difference approximations of the OGCM, except the continuity equation. Only the reference state is entirely physically relevant. The perturbed

states were designed with the sole objective of answering the question: ‘What would be the ventilation (or age distribution) under different conditions of velocity and diffusivity?’. This question arises from the need to evaluate the parameters of the leaky funnel representation.

Further developments based on the water age distribution [a generalisation of the age distribution function of Bolin and Rodhe (1973)] now offer the opportunity to revisit the leaky funnel model and eliminate concerns about possible biases stemming from the calibration method of MD08. Lifting concerns about the method of MD08 is essential in the purpose of pursuing our initial aim, which is to develop simple tools allowing to help understand differences in heat or gas uptake by different OGCMs in the context of climate change. As will be shown, the leaky funnel analogue has a potential for applications in modelling studies. It may help in evaluating the relative importance, at the largest scales of motion, of advection and diffusion in 3-D models.

Mixing is an essential mechanism in the ocean overturning circulation (Stommel and Arons, 1960a, b; Munk and Wunsch, 1998). Vertical mixing by working against the density gradient provides the necessary potential energy to sustain the deep circulation at its largest scale (Huang, 1999; Kuhlbrodt et al., 2007; Saenko et al., 2012). In most of the ocean interior, the vertical mixing is weak $\sim 10^{-5} \text{ m}^2 \text{ s}^{-1}$ (Ledwell et al., 1993; Toole and McDougall, 2001) but larger diapycnal diffusivities, up to $10^{-3} \text{ m}^2 \text{ s}^{-1}$, occur in very localised areas where tides and currents interact with the rough bottom topography (Polzin et al., 1997; Webb and Suginohara, 2001; Kunze et al., 2006; St. Laurent and Simmons, 2006). In OGCMs, diapycnal diffusivity plays an important role in determining the stability of the overturning circulation (Zhang et al., 1999; Schmittner and Weaver, 2001). An inadequate representation of the mixing processes in models may result in an unrealistic balance between the driving mechanisms of the deep ocean circulation and, consequently, to a possibly false assessment of the climatic feedbacks (Kuhlbrodt et al., 2007). According to Schmittner et al. (2009), the range in vertical mixing between models is a contributing factor to the large ranges in transient climate sensitivity and climate–carbon cycle feedbacks. Hence, it is of importance to be able to assess the mixing effectively taking place in models, i.e. including both numerical and explicit diffusivities. The leaky funnel model offers such a possibility.

The paper is organised as follows. After presenting the water age distribution function in Section 2, the analytical solutions for the leaky funnel are established in Section 3. We then perform numerical experiments with two 3-D OGCMs (Section 4). Section 5.1 is devoted to the calibration and the assessment of the leaky funnel model with respect to the 3-D OGCMs. Section 5.2 examines the

asymptotic behaviour of the global water age distribution and their interpretation. Section 5.3 reevaluates the leaky funnel characteristic scales in the light of numerical diffusivity and addresses the relevance of the leaky funnel model metrics. Conclusions are presented in Section 6.

2. Global water age distribution

As this work aims to assess ocean ventilation timescales, the focus here is on the water age distribution. This distribution naturally stems from the definition of the concentration distribution function (Deleersnijder et al., 2001; Delhez and Deleersnijder, 2002; Delhez et al., 2003) expressed for seawater. The concentration distribution function $c(t, \mathbf{x}, \tau)$ is defined so that $c(t, \mathbf{x}, \tau) \Delta \tau$, for $\Delta \tau \rightarrow 0$, represents the contribution of the material with an age that is in the interval $[\tau, \tau + \Delta \tau]$ to the total concentration¹ $C(t, \mathbf{x})$ at time t and position \mathbf{x} . $C(t, \mathbf{x})$ is then obtained from the integration of c in the age space. Since seawater is the aggregate of every constituent composing it, its concentration is equal to unity, $C(t, \mathbf{x}) = 1$. It automatically follows that its concentration distribution function c obeys the normalisation condition

$$C(t, \mathbf{x}) = \int_0^\infty c(t, \mathbf{x}, \tau) d\tau = 1 \quad (1)$$

The *mean water age* a is obtained from the first-order moment of the concentration distribution function (Delhez et al., 1999; Deleersnijder et al., 2001):

$$a(t, \mathbf{x}) = \frac{1}{C(t, \mathbf{x})} \int_0^\infty \tau c(t, \mathbf{x}, \tau) d\tau = \int_0^\infty \tau c(t, \mathbf{x}, \tau) d\tau. \quad (2)$$

Hence, $c(t, \mathbf{x}, \tau)$ is the distribution function for water age and will from now on be referred to as the *water age distribution*.

The *global water age distribution* results from the integration of $c(t, \mathbf{x}, \tau)$ over the volume Ω of the domain of interest:

$$\varphi(t, \tau) = \frac{1}{\Omega} \int_\Omega c(t, \mathbf{x}, \tau) d\Omega. \quad (3)$$

For $\Delta \tau \rightarrow 0$, $\Omega \varphi(\tau) \Delta \tau$ represents the volume of water with an age contained in the interval $[\tau, \tau + \Delta \tau]$. Expressions (3) and (1) lead to the following normalisation condition on φ :

$$\int_0^\infty \varphi(t, \tau) d\tau = 1. \quad (4)$$

The global water age distribution as given by eq. (3) is a generalisation of the age distribution function of Bolin and

Rodhe (1973), who restricted their study to steady-state problems. Furthermore, the global water age distribution is closely related to the *cumulative ventilation rate distribution* $\Phi(\tau)$ introduced in Primeau and Holzer (2006). In the case of a steady flow, $M\varphi(\tau) = \Phi(\tau)$, where M is the total mass of the fluid. The quantity $\Phi(\tau)$ having units of mass per unit time can be interpreted as the entering mass flux of surface waters that will reside in the interior for a time τ or longer before exiting (Primeau and Holzer, 2006; Hall et al., 2007).

On the other hand, $\varphi(\tau)$ is conceptually different from the *global distribution of mean water age* $\phi(a)$ examined in MD08. The latter represents a global inventory of water binned according to its steady-state mean age while the former is based on globally averaged transient ages. Computed directly with the mean water ages, $\phi(a)\Delta a$ represents the fraction of the volume occupied by water with mean ages included in the interval $[a, a + \Delta a]$. It takes the following form:

$$\phi(t, a) = \lim_{\Delta a \rightarrow 0} \frac{1}{\Omega \Delta a} \int_\Omega \square_{a, a+\Delta a}(a'(\mathbf{x})) d\Omega, \quad (5)$$

in which \square is the rectangular function:

$$\square_{a, a+\Delta a}(a') = \begin{cases} 1 & \text{if } a \leq a' \leq a + \Delta a, \\ 0 & \text{otherwise.} \end{cases} \quad (6)$$

Since the presence of diffusion generates differences in pathways towards the final location, a water parcel is characterised by a range of ages, rather than a single age. Therefore, when diffusion is active, $\phi(a)$ the global distribution of mean water age does not adequately represent the age distribution in the domain. On the other hand, $\varphi(\tau)$, which is based on the individual ages of the water parcel constituents, provides the correct domain age distribution. For both functions to be identical, it is necessary that the flow be purely advective. This point is further discussed in Section 5.1.

An additional quantity that will be of use further on is the domain-averaged mean water age. This *global mean water age* is identified with angle brackets and is related to φ by

$$\begin{aligned} \langle a(t) \rangle &= \frac{1}{\Omega} \int_\Omega a(t, \mathbf{x}) d\Omega = \frac{1}{\Omega} \int_\Omega \int_0^\infty \tau c(t, \mathbf{x}, \tau) d\tau d\Omega \\ &= \int_0^\infty \tau \varphi(t, \tau) d\tau. \end{aligned} \quad (7)$$

The global water age distribution is obtained by computing $c(t, \mathbf{x}, \tau)$ for the problem at stake and then integrating it over the domain. The equation governing the evolution of

¹ C represents a mass fraction, i.e. the ratio of the total mass of the constituent in the sample to the total mass of the sample.

$c(t, \mathbf{x}, \tau)$ is (Delhez et al., 1999; Deleersnijder et al., 2001; Delhez and Deleersnijder, 2002)

$$\frac{\partial c}{\partial t} = -\nabla \bullet (\mathbf{u}c - \mathbf{K} \bullet \nabla c) - \frac{\partial c}{\partial \tau}, \quad (8)$$

with \mathbf{u} the velocity vector and \mathbf{K} the diffusivity tensor, which must be symmetric and positive definite (Deleersnijder et al., 2001).

In the context of ocean ventilation studies, solutions to eq. (8) are sought by tagging water masses exposed to the surface with unit concentration and zero mean age. This is achieved through imposing that at the ocean surface S

$$c(t, \mathbf{x}, \tau) = \delta(\tau), \text{ for } \mathbf{x} \in S, \quad (9)$$

where δ is the Dirac function, i.e. $\delta(\tau - \tau') = 0$ when $\tau \neq \tau'$ with δ satisfying the identity $\int_{-\infty}^{\infty} \delta(\tau) d\tau = 1$.

3. Leaky funnel solutions

In this text, we restrict the description of the leaky funnel to its key aspects. The interested reader will find a detailed description of this model together with the mathematical expressions and derivations of analytical solutions in MD08.

The leaky funnel (Fig. 1) is a semi-infinite pipe characterised by a cross-sectional area $S(x)$, which is a decreasing function of x , the downstream coordinate ($0 \leq x < \infty$). Both advection and diffusion processes contribute to the transport in the funnel. The porous outer envelope allows water to escape the domain while being transported downstream. Assuming further that all variables and properties are homogeneously distributed over S , i.e. they solely depend on x and t , yields a 1-D problem.

In this configuration, the evolution of the water age distribution $c(t, x, \tau)$ in the leaky funnel obeys

$$S \frac{\partial c}{\partial t} + \frac{\partial(SUc)}{\partial x} = -Qc + \frac{\partial}{\partial x} \left(SK \frac{\partial c}{\partial x} \right) + S \frac{\partial c}{\partial \tau}, \quad (10)$$

with U and K the velocity and the diffusivity, respectively, and where $Q(t, x)$ represents the water flux leaving the funnel through the porous lateral boundary. This flux is obtained from the continuity equation, which reads

$$\frac{\partial(SU)}{\partial x} = -Q. \quad (11)$$

In order to obtain analytical solutions, we take U and K as positive constants and assume that all variables are at a steady state. We also impose that the funnel section decreases exponentially with a constant length scale L : $S(x) = S_0 \exp(-x/L)$.

Under these assumptions, eq. (10) reduces to the classical 1-D problem of advection and diffusion in a semi-infinite pipe with a constant section:

$$\frac{\partial c}{\partial \tau} = -U' \frac{\partial c}{\partial x} + K \frac{\partial^2 c}{\partial x^2}. \quad (12)$$

The modified velocity $U' = U + K/L$ arises from the section change with x .

We solve eq. (12) by imposing condition (9) at the funnel entrance, $c(x = 0, \tau) = \delta(\tau)$, together with the additional constraints

$$c(x, \tau = 0) = 0, \text{ and } c(x = \infty, \tau) = 0. \quad (13)$$

The solution to eq. (12) under such conditions is found to be (e.g. Hall and Haine, 2002; Delhez et al., 2003)

$$c(x, \tau) = \frac{x}{\sqrt{4\pi K \tau^3}} \exp \left[-\frac{(x - U'\tau)^2}{4K\tau} \right]. \quad (14)$$

The leaky funnel domain is semi-infinite but its volume is finite ($\Omega = \int_0^\infty S(x) dx = S_0 L$); therefore, domain-averaged quantities may be computed.

The global water age distribution, obtained by integrating eq. (14) over Ω , is given by the following expression:

$$\begin{aligned} \varphi(\tau) &= \frac{1}{L} \int_\Omega e^{-x/L} c(x, \tau) dx = \sqrt{\frac{K}{\pi L^2 \tau}} \exp \left(-\frac{U'^2}{4K} \tau \right) \\ &+ \frac{1}{\theta} \left[1 + \operatorname{erf} \left(\frac{1}{\theta} \sqrt{\frac{L^2}{K}} \tau \right) \right] \exp \left(-\frac{U}{L} \tau \right), \end{aligned} \quad (15)$$

in which

$$\frac{1}{\theta} = \frac{1}{2} \left(\frac{U}{L} - \frac{K}{L^2} \right), \text{ and } \operatorname{erf}(y) = \frac{2}{\sqrt{\pi}} \int_0^y e^{-\xi^2} d\xi.$$

To get the global water age distribution [eq. (15)] as well as forthcoming expression [eq. (16)], integrals involving the water age distribution have to be performed, a task that may be achieved with the help of Gradshteyn and Ryzhik (2000) or a symbolic calculation software.

The normalisation condition (4) for $\varphi(\tau)$ holds true, as is demonstrated in Appendix A.

The mean water age is found to be

$$a(x) = \int_0^\infty \tau c(x, \tau) d\tau = \frac{x}{U'}. \quad (16)$$

The global mean water age or domain-averaged water age $\langle a \rangle$ is given by the timescale L/U' :

$$\langle a \rangle = \Omega^{-1} \int_0^\infty a(x) S(x) dx = \int_0^\infty \tau \varphi(\tau) d\tau = \frac{L}{U'}. \quad (17)$$

4. 3-D OGCM experiments

In order to test the leaky funnel representation, we perform numerical experiments with the help of two OGCMs. Besides the annual mean circulation from the Louvain-la-Neuve OGCM (UL-OM) (Deleersnijder and Campin, 1995; Campin and Goosse, 1999), which we utilised in MD08, we also take 3-D fields provided by the dynamical Large-Scale Geostrophic Ocean General Circulation Model (LSG-OM) (Maier-Reimer et al., 1993) in its annually averaged version (Winguth et al., 1999; Heinze et al., 2003). A description of the main characteristics of these OGCMs is given in Appendix B.

At a steady state, eq. (8) reduces to the usual equation describing the evolution of concentration in which time is replaced by τ :

$$\frac{\partial c}{\partial \tau} = -\nabla \bullet (\mathbf{u}c - \mathbf{K} \bullet \nabla c). \quad (18)$$

The steady-state water age distribution can, thus, be obtained as the transient solution of a classical advection–diffusion problem (Beckers et al., 2001; Delhez and Deleersnijder, 2002).

Equation (18) is solved numerically with the same transport scheme as that used for tracers in the 3-D model. Advective and diffusive fluxes across the ocean floor and lateral boundaries are set to zero. We impose homogeneous initial conditions: $c(\mathbf{x}, \tau = 0) = 0$ for \mathbf{x} belonging to the ocean domain.

At the ocean surface S , the boundary condition should be given by eq. (9) rewritten for steady state

$$c(\mathbf{x}, \tau) = \delta(\tau), \text{ for } \mathbf{x} \in S. \quad (19)$$

For a stationary problem, c is therefore the impulse response or Green’s function (Beckers et al., 2001).

There are, however, technical difficulties linked to the use of a Dirac impulse as boundary condition. In order to circumvent these, we take advantage of the fact that the impulse response may be obtained from the derivative of the step response. Indeed, the delta function can be viewed as the derivative of the unit or Heaviside step function, $dH(\tau)/d\tau = \delta(\tau)$ ($H(\tau) = 1$ for $\tau \geq 0$ and $H(\tau) = 0$ for $\tau < 0$). We then numerically solve eq. (18) for a function, which we denote as c^* . This solution is obtained under the same constraints as applied to c (homogeneous initial conditions and no flux across the boundaries) at the exception of the boundary condition at the ocean surface, which for c^* is given by

$$c^*(S, \tau) = H(\tau). \quad (20)$$

The derivative with respect to τ of c^* yields the water age distribution in the 3-D model. One finally obtains the global water age distribution (Fig. 2) by

computing the domain-average of $c(\mathbf{x}, \tau)$ at each time step.

5. Results and discussion

5.1. Characteristic scales

The parameters needed to fully determine the leaky funnel distribution (15) may be deduced by fitting this expression to the data resulting from the 3-D OGCM experiments. For this purpose, it is necessary to identify independent parameters. Two distinct timescales stem from a close examination of the parameters intervening in eq. (15): $A_0 = L/U$ and $A_D = L^2/K$, i.e. the advection and diffusion timescales characterising the flow. Reexpressing eq. (15) by means of the definitions for A_0 and A_D leads to

$$\begin{aligned} \varphi(\tau) = & \sqrt{\frac{1}{\pi A_D \tau}} \exp \left[-\frac{1}{4A_D} \left(1 + \frac{A_D}{A_0} \right)^2 \tau \right] \\ & + \frac{1}{\theta} \left[1 + \operatorname{erf} \left(\frac{1}{\theta} \sqrt{A_D \tau} \right) \right] \exp \left(-\frac{\tau}{A_0} \right), \quad (21) \\ \text{and } \frac{1}{\theta} = & \frac{1}{2} \left(\frac{1}{A_0} - \frac{1}{A_D} \right). \end{aligned}$$

We are hence left with two parameters to be determined, A_0 , and A_D .

The non-linear least squares fitting procedure in IDL MPFIT (Markwardt, 2009) based on the Levenberg-Marquardt algorithm (Moré, 1978) is used to evaluate those two parameters from the OGCM global water age distribution. In order to prevent large values at very low ages to dominate the solution, we specify weights to the OGCM results inversely proportional to the function values.² The OGCM responses were computed from simulations performed over 20000 years.

Table 1 presents the values of A_0 and A_D obtained with this method, together with the estimated Peclet number and global mean water age $\langle \hat{a} \rangle$:

$$Pe = \frac{UL}{K} = \frac{A_D}{A_0}, \quad (22)$$

$$\langle \hat{a} \rangle = \frac{L}{U'} = \left(\frac{1}{A_0} + \frac{1}{A_D} \right)^{-1}. \quad (23)$$

It should not be immediately concluded from the values in Table 1 that the transport in LSG-OM is less diffusive than

²We tested this method by also considering weights linearly increasing with τ or by using the square root of the function. Those methods produce results which are extremely close to those presented herein.

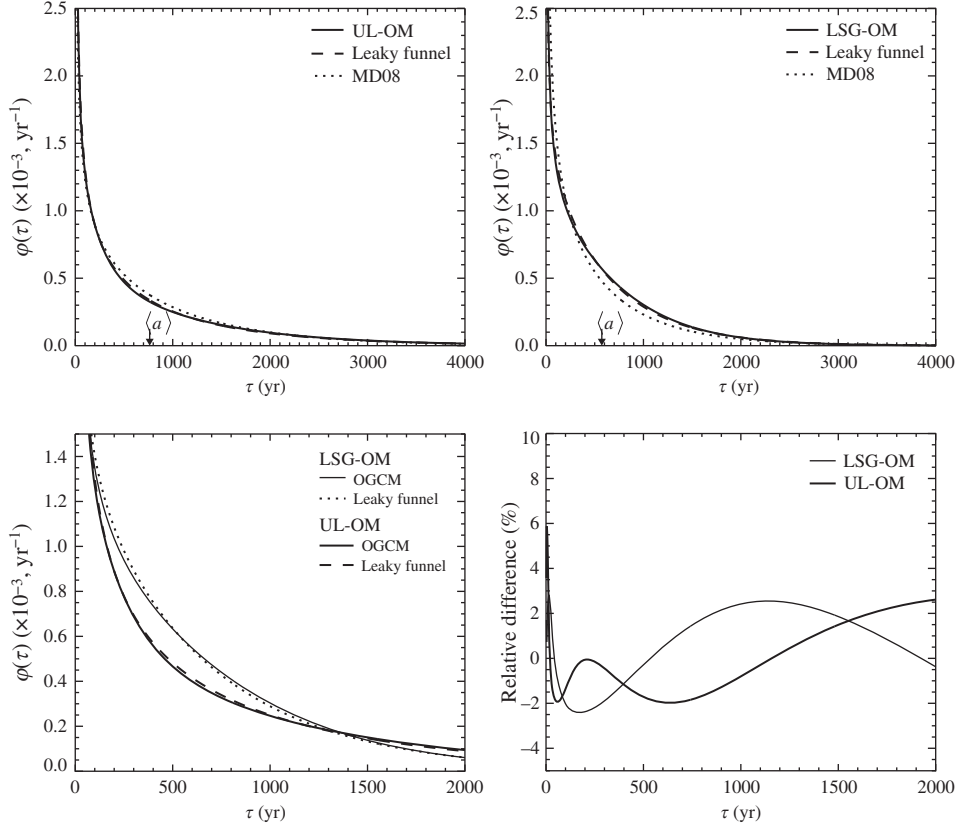


Fig. 2. Global water age distribution ϕ (solid line) versus age in two 3-D OGCMs, UL-OM (top left) and LSG-OM (top right), compared to that predicted by the leaky funnel (dashed line). The leaky funnel curve in each panel is obtained with the parameters appropriate to the corresponding OGCM from Table 1. In the two upper panels, the curve computed with the parameters as estimated by the method of MD08 is also represented (dotted line). The arrow in those two panels points to the actual global mean water age $\langle a \rangle$ obtained with each OGCM. The lower two panels allow the comparison of both OGCMs with focus on ages under 2000 years. Global water age distribution ϕ (bottom left) as obtained with LSG-OM (thin solid) and UL-OM (thick solid) and as estimated by the leaky funnel for each OGCM: LSG-OM (dotted) and UL-OM (dashed). Relative difference (bottom right) between the OGCM and the leaky funnel global water age distributions for LSG-OM (thin solid) and UL-OM (thick solid).

in UL-OM. As will be shown in Section 5.3, this is an artefact due to the neglect of numerical diffusion in eq. (21). Actually, the effective Pe of both models is of the same order of magnitude.

As can be seen from Table 1, the concordance between estimated and actual OGCM global mean water ages is excellent. Further, there is a fair agreement between the experimental (OGCM) and theoretical (leaky funnel) curves (Fig. 2). Figure 2 also contains the distribution given by eq. (21) but in which we imposed the parameters as obtained with the MD08 method.

The differences between the curve resulting from the present work and that produced by the MD08 method may be explained by several factors. The least-squares fitting procedures of MD08 and of the present work are performed with the help of series containing quite different information: in MD08, the series represents steady-state globally averaged ages while, in the present work, it

consists of global average of transient ages. Hence, the parameter values obtained with the MD08 method principally reflect the deep ocean properties (since it occupies the largest volume and since the upper layers are characterised by both small age and volume). On the contrary, the global water age distribution contains information at all ages. Despite the fact that we give more weight to older ages, the parameters estimated with the help of ϕ are significantly influenced by younger ages. Hence, those estimates are affected by characteristics of well-ventilated ocean areas usually associated to a larger vertical diffusivity in OGCMs. The heterogeneity of the OGCM regional dynamics also contributes to the differences between the two curves. In addition, as exposed further in the text, the two OGCMs differ with respect to the relative role played by advection and diffusion (including numerical diffusion) in setting their ventilation rate. This might be the reason for the different behaviour of the MD08 curve with respect to

Table 1. Parameters A_0 and A_D of the leaky funnel model as obtained from a least squares fit to the 3-D model results

OGCM	A_0 (yr)	A_D (yr)	Pe	$\langle \hat{a} \rangle$ (yr)	$\langle a \rangle$ (yr)
UL-OM	1243	1982	1.6	764	764
LSG-OM	644	5249	8.1	574	573

The estimated Pe number and global mean water age are given in columns 4 and 5, respectively. The last column contains the actual global mean water age from the 3-D OGCM experiment.

$\varphi(\tau)$ in the UL-OM and LSG-OM cases. Nevertheless, the similarity of the distributions obtained with the MD08 method and in the present work adds confidence to the conclusions of MD08 as well as to the ability of the leaky funnel at capturing properties of the deep-ocean ventilation as computed by OGCMs.

Previous research has focussed on characterising the local age distribution in terms of a parametric model based on the solution of 1-D advection-diffusion equation in a semi-infinite domain, (i.e. an inverse Gaussian distribution). Peacock and Maltrud (2006) compared the inverse Gaussian function to distributions computed from an OGCM and documented regions where systematic biases occurred, including regions of multimodality in the Southern Ocean. Here, we focus on the global water age distribution, a monotonically decreasing function, which is more amenable to being described in terms of a simple parametric model. The asymptotic analysis of the next section shows that the leaky funnel is able to capture OGCMs global water age distribution at both low and large ages.

5.2. Asymptotic analysis

The asymptotic properties of the global distribution may provide some insight into ocean processes as reproduced by OGCMs. Two regimes are identified considering the behaviour of φ at low or large ages.

For $\tau \rightarrow 0$, solution (21) behaves like

$$\varphi(\tau) \sim \frac{1}{\sqrt{\pi A_D \tau}}, \quad (24)$$

an expression that does not involve advection. Diffusion is the main process controlling the distribution for $\tau \rightarrow 0$. As opposed to advection, which has a finite propagation speed, the parabolic nature of diffusion transmits the initial perturbation at once to areas far from the boundary. Hence, in the early stages, regions rapidly exchanging with the surface dominate the solution. This feature is made clear in Fig. 3 where it is seen that the global water age distribution closely follows eq. (24) for ages that are typical of newly formed water masses.

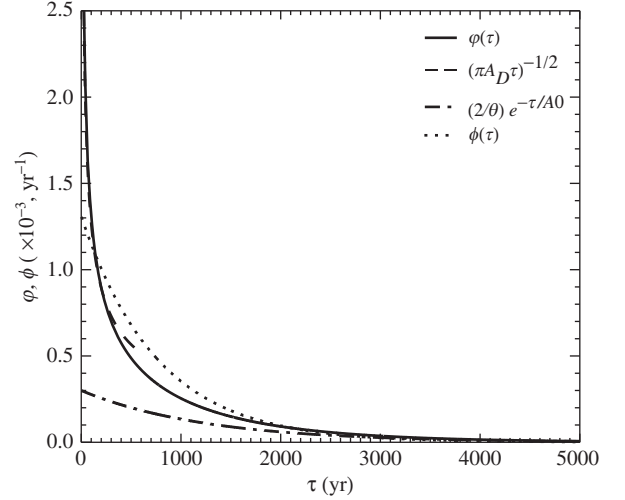


Fig. 3. Global water age distribution $\varphi(\tau)$ in the leaky funnel (solid line) versus age. The two asymptotes when $\tau \rightarrow 0$ and $\tau \rightarrow \infty$ are represented by the dashed and dotted-dashed lines, respectively. Also illustrated is the global distribution of mean water age $\phi(\tau)$ (dotted line). We build these curves with the help of the A_0 and A_D values obtained with the UL-OM model.

The $\tau^{-1/2}$ singularity of $\varphi(\tau)$ at $\tau = 0$ is a physical consequence of diffusion (Primeau and Holzer, 2006; Hall et al., 2007). This singularity reflects the fact that the gross (one-way) flux into the interior is infinite as it is dominated by fluid elements that reside in the interior for infinitesimally short times before they make contact with the surface and exit the domain. A simple random walk model is presented in Hall and Holzer (2003) to illustrate the phenomenon.

The role of diffusion also explains the discrepancy between the global distribution of mean age ϕ and φ (Fig. 3). For the leaky funnel, as established in MD08 (see also Appendix D), ϕ takes the form:

$$\phi(a) = \frac{e^{-a/\langle \hat{a} \rangle}}{\langle \hat{a} \rangle}. \quad (25)$$

ϕ is computed with the help of the global mean water age, that is an equilibrium age reflecting mostly the deep ocean properties. Only in the case of negligible diffusion does ϕ correctly approximate φ . Indeed, if $K \rightarrow 0$, then φ reduces to

$$\varphi(\tau) \sim \frac{e^{-\tau/A_0}}{A_0}, \quad (26)$$

which is equivalent to eq. (25) since $\langle a \rangle \rightarrow A_0$ when $K \rightarrow 0$.

For large ages, φ may be approximated by

$$\varphi(\tau) \sim (2/\theta)e^{-\tau/A_0}, \quad \text{for } \tau \rightarrow \infty. \quad (27)$$

This distribution is identical to that characterising a first-order removal process (Bolin and Rodhe, 1973) with an

e-folding decay given by the advection time scale A_0 . A_0 being a constant the removal rate is identical for all ages. Hence, above some age, the probability to escape the main flow is the same for all particles, whatever their age.

The fact that both the leaky funnel and the OGCMs behave as first-order removal processes for $\tau \rightarrow \infty$ is a consequence of the finite volume of their domains, which ensures that the advection–diffusion transport operators have discrete eigenmode expansions. In the limit $\tau \rightarrow \infty$, solutions are dominated by the most slowly decaying eigenmode (Haine and Hall, 2002; Primeau and Holzer, 2006; Primeau and Deleersnijder, 2009). The least-squares fit of the leaky funnel model parameters to the OGCMs’ global water age distribution for ages ranging from zero to more than 20000 years ensured a close correspondence of the most slowly decaying eigenvalues for the OGCMs and the leaky funnel model. Indeed, if the least-squares fit had been performed over an infinite age interval the dominance of the solution by the most slowly decaying eigenmode for large ages would have ensured exact equality between the advective timescale A_0 for the leaky funnel model and the reciprocal of the most slowly decaying eigenmode of the OGCMs’ advection-diffusion transport operator subject to Dirichlet boundary conditions.

The age distribution as computed here also provides information on the adjustment after a sudden change in the system. The analysis of the leaky funnel approximation suggests the existence of two regimes in the response of ocean water masses. The amount of very young particles is very large, indicating a fast exchange with the boundary. This results in the rapid initial decrease in the adjustment. As age (or time) progresses, a longer time scale controls the distribution. The response or adjustment time of the interior ocean as a whole is then given by A_0 , the eigenmode with smallest absolute value.

5.3. Appraisal of leaky funnel metrics

It is of importance to assess the mixing effectively taking place in models, i.e. including both numerical and explicit diffusivities. Explicit diffusion has a clear physical meaning. It is meant to take into account unresolved subgridscale physical processes. On the contrary, numerical diffusion, associated to the advection scheme, is a consequence of the finite difference method and does not bear any physical significance. However, its effects should not be overlooked. Indeed, it seems that, in ocean models, the numerical diffusivity of advection schemes is often of the same order of magnitude as the explicit one (Kuhlbrodt et al., 2007). Such numerical artefacts bear consequences to the simulated tracer distributions (Oschlies, 2000; Doney et al., 2004).

However, assessing the actual numerical diffusion magnitude in OGCMs is not always straightforward (e.g. Burchard and Rennau, 2008). The leaky funnel model on the other hand offers such a possibility. The estimates of both the explicit and numerical diffusivities, together with the advective time scale, allow then to characterise the transport in individual OGCM. At this stage, it is important to mention that our aim is not to assess the OGCMs used in this work but to evaluate the relevance of the information provided by the leaky funnel representation in the purpose of providing metrics for model appraisal.

Extracting any information about the numerical diffusion from the global water age distribution proves to be a very complex and intricate task. On the other hand, the method from MD08 allows such a derivation. Since the present work corroborates the results from MD08, the latter approach can be used to derive the leaky funnel parameters and assess the role of numerical diffusion in OGCMs. Further, as commented on in MD08 and detailed in Appendix C, ignoring the role played by numerical diffusivity results in an overestimate of A_D and, since eq. (23) holds, in an underestimate of A_0 .

The effective Peclet number to be associated to the transport in the OGCMs takes into account both the explicit and numerical diffusivities. It is given by

$$\frac{1}{Pe} = \frac{K^E + K^N}{UL} = \frac{1}{Pe^E} + \frac{1}{Pe^N}, \quad (28)$$

where $Pe^E = UL/K^E$ and $Pe^N = UL/K^N$ represent the Peclet numbers associated with the explicit K^E and numerical diffusivity K^N , respectively.

The leaky funnel parameters corresponding to UL-OM were already determined by MD08. In the same way we performed $M=21$ experiments with the LSG-OM, in which the velocity and explicit diffusivity were homogeneously multiplied by constant factors (comprised in [1.,8.] and [0.125,1.], for the explicit diffusivity and the velocity, respectively). A least-squares fit to the 21 OGCM domain-averaged ages provides estimates of the leaky funnel parameters $\{A_0, Pe^E, Pe^N\}$ corresponding to LSG-OM. These values as well as those for UL-OM from MD08 are given in Table 2. The agreement between ages predicted by the leaky funnel and those from the LSG-OM is not illustrated here but is very good with correlation coefficients close to 1.

The two models differ drastically in their advection timescales A_0 . As discussed earlier, the A_0 scale represents the adjustment time to a perturbation or the most slowly decaying mode of the OGCMs’ transport operator. UL-OM is characterised by a larger A_0 value, which translates in a longer timescale for anthropogenic CO_2 uptake relative to LSG-OM (Fig. 4). This is a consequence of the more

Table 2. Parameters of the leaky funnel model as obtained from a least squares fit to the domain-averaged water ages resulting from several experiments with two 3-D models (UL-OM, column 2, and LSG-OM, column 3)

	UL-OM	LSG-OM
A_0 (yr)	1010	690
Pe^E	6.4	14.0
Pe^N	7.0	2.8
Pe	3.3	2.4
A_D (yr)	3333	1656

The values in this Table are obtained by the MD08 method with numerical diffusion explicitly considered. Line 4 gives the effective Peclet number computed from eq. (28) and the last line contains the effective A_D scale ($A_D = Pe A_0$).

sluggish circulation and longer pathways in the Pacific Ocean predicted by UL-OM with respect to LSG-OM. In the Pacific Ocean, the longer advection timescale characterising UL-OM is consistent with larger trajectories resulting in older, more radiocarbon-depleted water masses in comparison with the LSG-OM (Fig. 5). The more vigorous circulation in LSG-OM translates into less radiocarbon-depleted water masses in that area.

The role played by numerical diffusion in the transport is made clear from the values in Table 2. These values are in agreement with the OGCMs mathematical formulation and numerical scheme. Indeed, numerical diffusion is congruent with the upstream scheme used for resolving advection in LSG-OM both along the horizontal and the vertical. The use of explicit diffusion in that model is restricted to

convective processes in addition to a small horizontal term preventing mode divergence due to the use of an E-grid (Appendix B). Hence, numerical diffusion contributes most to the effective diffusion in that model.

In contrast, UL-OM makes use of a less diffusive numerical scheme for advection. This explains the larger Pe^N with respect to LSG-OM, while the generalised use of explicit diffusion translates into a lower Pe^E . Though the global, or effective, Peclet numbers associated to each model are very close (line 4 in Table 2), the underlying mechanisms are very different. The difference in the mechanisms controlling the mixing results in contrasted tracer vertical distributions (Fig. 5). Indeed, the vertical profiles of tracers in the Atlantic Ocean predicted by LSG-OM are much smoother than those obtained with UL-OM. The Peclet numbers associated to the interior circulation appear to be rather low. Other studies also pointed to the possibility that the large scale transport in the ocean might be more dominated by diffusion than previously thought (Deleersnijder et al., 2002; Holzer and Primeau, 2006). However, these conclusions result from experiments with coarse grids OGCMs. Reassessing them by means of eddy-resolving models would be necessary.

The results in Table 2 contrast with the figures presented in Table 1. Two factors contribute to these differences. First, the results presented in Table 2 are obtained with the help of the global mean water ages, which mostly reflect the deep ocean properties. In contrast, the global water age distribution contains information spanning all ages. The parameter estimates based on the latter is hence significantly affected by near surface and convective mixing processes, yielding lower Pe numbers than those predicted with the help of the MD08 method when numerical diffusion is not considered (compare values in Table 1 to those in the lower half of Table 3). Second, it has not been possible to extract any information on numerical diffusion from the global water age distribution. On the contrary, the MD08 method allows to discriminate between explicit and numerical diffusivities. As detailed in Appendix C, neglecting the contribution from numerical diffusion in the least squares fitting procedure does not bear any consequences on the goodness of the fit for water ages. Omitting it, however, results in biased estimates of A_0 and Pe ; A_0 is moderately underestimated while A_D (hence Pe) is significantly overestimated.

It is noteworthy that A_0 appears to be comparatively less affected by the method used to estimate it than A_D , hence Pe (Tables 1 and 2). A_0 being the timescale characterising the global water age distribution for large ages (eq. 27), it is expected that estimating that timescale with the help of $\varphi(\tau)$ or by the MD08 method would result in similar values, since the latter method is based on domain averaged ages, which implicitly give more weight to the larger ages

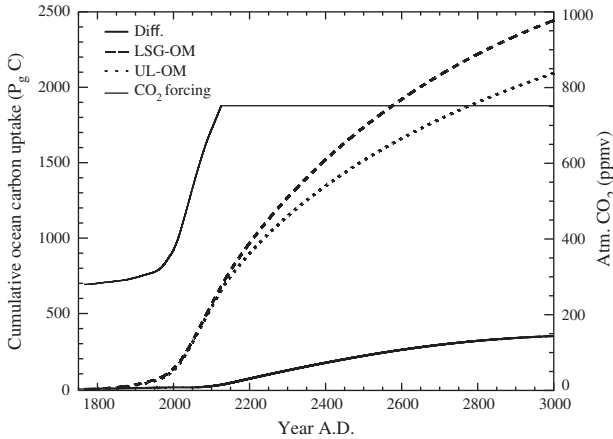


Fig. 4. Difference in CO_2 cumulative uptake (thick solid line) by two ocean global carbon models. The individual uptakes (represented as anomalies with respect to 1765 A.D.) are obtained from abiotic constrained CO_2 experiments with LSG-OM (dashed line) and UL-OM (dotted line). The thin solid line corresponds to the atmospheric CO_2 forcing used in these experiments. Units for the atmospheric CO_2 are given on the right axis.

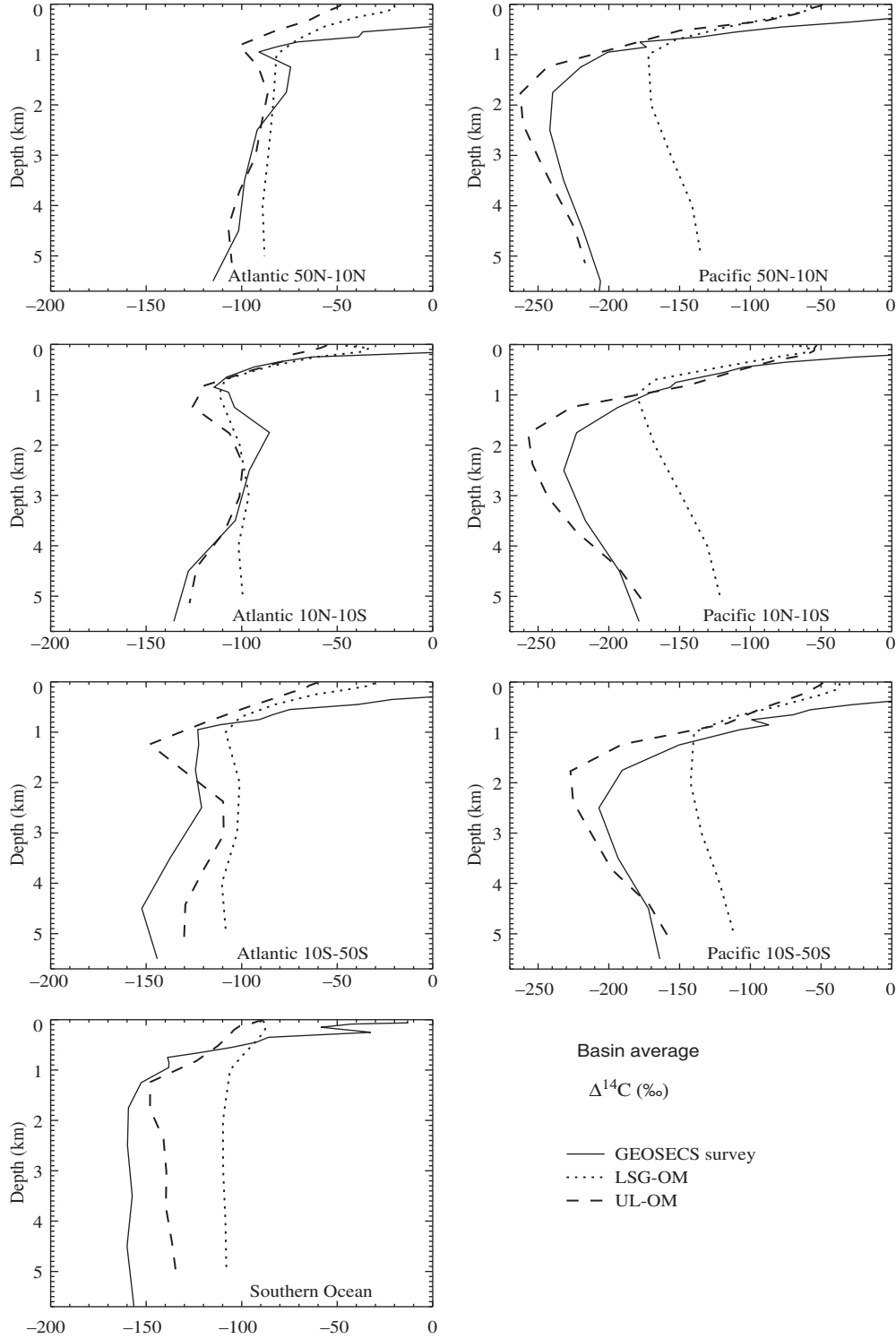


Fig. 5. Mean $\Delta^{14}\text{C}$ vertical profiles in several ocean basins from GEOSECS (solid lines; Stuiver et al., 1981) and from two pre-industrial experiments with the OGCM standard versions UL-OM (dashed lines) and LSG-OM (dotted lines). The values in the North, Equatorial and Southern Atlantic and Pacific Oceans are reproduced, respectively, in the upper left and right three panels, with the bottom panel representing the Southern Ocean (south of 50°S). The pre-industrial OGCM $\Delta^{14}\text{C}$ is computed with the simplified method of Toggweiler et al. (1989). The discrepancy between models and data in the upper ocean partly results from the penetration of bomb ^{14}C that is not considered in these numerical experiments.

Table 3. Best fit parameters of the leaky funnel when numerical diffusion is considered (rows 4 and 5) or not (rows 7 and 8) in the least squares fitting procedure of MD08

OGCM	A_0 (yr)	Pe^E	Pe^N	Pe	$\langle \hat{a} \rangle$ (yr)	$\langle a \rangle$ (yr)
Numerical diffusion considered						
UL-OM	1010	6.4	7.0	3.3	778	764
LSG-OM	690	14.0	2.8	2.4	485	573
Numerical diffusion neglected						
UL-OM	884	7.3	—	7.3	778	764
LSG-OM	511	18.9	—	18.9	485	573

For each OGCM (column 1), this table gives the advective timescale (column 2), the Peclet numbers associated to the explicit and numerical diffusivities (columns 3 and 4) and the effective Pe (column 5). Column 6 contains the estimated domain averaged water age $\langle \hat{a} \rangle$ computed from eq. (23) with the help of A_0 and Pe in the present table. The global mean age predicted by the standard version of the OGCMs (that is, for $\beta_i = \gamma_i = 1$) is given in column 7.

characterising the deep ocean. The MD08 method is probably more appropriate in the purpose of assessing the characteristics of the deep ocean circulation as reproduced by OGCMs. First, the figures obtained with this method are less influenced by surface processes since it relies on global mean water ages. Second, it allows to extract pertinent information on the relative roles of numerical and explicit diffusivities in setting the distribution of tracers in OGCMs.

6. Conclusion

The method of MD08 was questionable since it disregards the OGCM internal dynamics. The present work allows to alleviate such concerns by using a different concept, the global water age distribution. The good correlation between the age distributions in the leaky funnel and in the OGCMs provides a further assessment of the leaky funnel. This assessment is performed in a way that is fully coherent with the OGCM dynamics.

The leaky funnel representation seems able to capture not only the mean water ages (Mouchet and Deleersnijder, 2008) but also, as demonstrated in this work, the global water age distribution predicted by two different OGCMs. One conclusion of this work is that the deep ocean in coarse grid OGCMs seems to behave as first-order removal process for large ages with an e-folding timescale given by the advective timescale A_0 . This timescale for the leaky funnel model may be related to the reciprocal of the most slowly decaying eigenmode of the OGCMs advection-diffusion transport operator subject to Dirichlet boundary conditions.

The leaky funnel model provides analytical solutions that are simple to deal with, making it possible to obtain

characteristic scales of the deep-ocean circulation as reproduced by OGCMs. It also provides a simple mean to evaluate the relative roles of advection and diffusion in complex OGCMs. Furthermore, it offers the possibility to evaluate the extent to which numerical diffusion affects this circulation. The values provided by the leaky funnel appear to be fully coherent with the OGCMs' physics and numerics. Although a 1-D model may not always provide a pertinent representation of the complex 3-D circulation (Olbers and Wenzel, 1989), there are many examples of reduced-dimension models that proved highly successful at helping interpret the results from much more complex models (e.g. Deleersnijder et al., 1997; Tartinville et al., 1997; Deleersnijder et al., 1998).

We are aware that, up to now, the leaky funnel has only been tested with coarse grid OGCMs. Testing it against 3-D models with increased resolution and more detailed vertical mixing would perhaps be necessary before generalising the conclusions of this analysis. Further, the fact that the information provided is exclusively global, representing a spatially integrated measure of heterogeneously distributed processes, may constitute a limitation in its use.

7. Acknowledgements

We are grateful to Arne Winguth, Ernst Maier-Reimer and Jean-Michel Campin for kindly providing the 3-D OGCM transport fields. Jim Orr and an anonymous reviewer helped much improving the manuscript. Eric Deleersnijder is a honorary Research Associate with the Belgian Fund for Scientific Research (F.R.S. – FNRS). François Primeau was supported by NSF grant OCE-0928395.

8. Appendix A: proof that $\varphi(\tau)$ as given by eq. (15) verifies the normalisation condition (4)

The integration of eq. (15) is made easier by first rewriting it as follows:

$$\begin{aligned} \varphi(\tau) = & \sqrt{\frac{K}{\pi L^2 \tau}} \exp\left(-\frac{U'^2 \tau}{4K}\right) + \frac{1}{\theta} \exp\left(-\frac{U\tau}{L}\right) \\ & + \frac{1}{\theta} \operatorname{erf}\left(\frac{1}{\theta} \sqrt{\frac{L^2 \tau}{K}}\right) \exp\left(-\frac{U\tau}{L}\right). \end{aligned} \quad (\text{A1})$$

We treat separately the integration of each of the three terms on the right-hand side of eq. (A1).

The integration of the first term is performed with the help of $\int_0^\infty y^n \exp(-ay) dy = \frac{\Gamma(n+1)}{a^{n+1}}$ (Abramowitz and

Stegun, 1972) in which we set $n = -1/2$ and $a = U'^2/(4K)$. Since $\Gamma(1/2) = \sqrt{\pi}$, we get

$$\sqrt{\frac{K}{\pi L^2}} \int_0^\infty \tau^{-1/2} \exp\left(-\frac{U'^2 \tau}{4K}\right) d\tau = \frac{2K}{LU'}. \quad (\text{A2})$$

The integration of the second term is straightforward

$$\int_0^\infty \frac{1}{\theta} \exp\left(-\frac{U\tau}{L}\right) d\tau = \frac{L}{U\theta}. \quad (\text{A3})$$

For the treatment of the last term, we take advantage of the following properties of the error function:

$$\frac{d}{dy} \text{erf}(y) = \frac{2}{\sqrt{\pi}} \exp(-y^2), \quad \text{erf}(0) = 0 \text{ and } \text{erf}(\infty) = 1.$$

We then make use of the integration by parts relationship $\int f(\tau)g'(\tau)d\tau = f(\tau)g(\tau) - \int f'(\tau)g(\tau)d\tau$. Setting $f = \text{erf}\left(\frac{1}{\theta}\sqrt{\frac{L^2\tau}{K}}\right)$ and $g' = \exp\left(-\frac{U\tau}{L}\right)$, it follows:

$$f' = \frac{1}{\theta} \sqrt{\frac{L^2}{K\pi}} \tau^{-1/2} \exp\left(-\frac{L^2\tau}{K\theta^2}\right)$$

and

$$g = -\frac{L}{U} \exp\left(-\frac{U\tau}{L}\right).$$

The integral then becomes

$$\begin{aligned} & \int_0^\infty \frac{1}{\theta} \text{erf}\left(\frac{1}{\theta}\sqrt{\frac{L^2\tau}{K}}\right) \exp\left(-\frac{U\tau}{L}\right) d\tau = -\frac{L}{\theta U} \\ & \times \left[\text{erf}\left(\frac{1}{\theta}\sqrt{\frac{L^2\tau}{K}}\right) \exp\left(-\frac{U\tau}{L}\right) \right]_0^\infty + \frac{L^2}{U\theta^2\sqrt{K\pi}} \int_0^\infty \tau^{-1/2} \\ & \times \exp\left(-\left(\frac{U}{L} + \frac{L^2}{K\theta^2}\right)\tau\right) d\tau = \frac{L^2}{U\theta^2} \frac{\Gamma(1/2)}{\sqrt{K\pi}} \frac{1}{\sqrt{\frac{U}{L} + \frac{L^2}{K\theta^2}}} \\ & = \frac{L^2}{U\theta^2} \frac{1}{\sqrt{\frac{UK}{L} + \frac{L^2}{\theta^2}}}. \end{aligned} \quad (\text{A4})$$

Adding together eqs. (A2), (A3) and (A4), one easily gets that eq. (15) verifies condition (4).

9. Appendix B: main features of the OGCMs used in this study

The transport model is driven by 3-D fields of velocity components, potential temperature, salinity and convective mixing from two OGCMs in their annually averaged versions. The numerical scheme of the offline transport model is adapted according to the OGCM fields driving it so that the physics determining the distribution of tracers is

as close as possible to that determining the distribution of active variables in the dynamical model. Both these models belong to the coarse-grid OGCM class as none of them is eddy-resolving. They, nevertheless, capture the essential of deep ocean circulation. A short description of both OGCMs follows:

- **UL-OM** (Deleersnijder and Campin, 1995; Campin and Goosse, 1999): UL-OM is a primitive-equation, free-surface OGCM resting on the usual set of assumptions, i.e. the hydrostatic equilibrium and the Boussinesq approximation. The horizontal resolution is $3^\circ \times 3^\circ$. The so-called ‘z-coordinate’ underlies a vertical discretisation with 15 levels ranging in thickness from 20 m at the surface to 700 m in the deep ocean. A realistic bathymetry is used. The parameterisation of vertical mixing is based on the Pacanowski and Philander (1981) formulation. Wherever the vertical density profile is unstable, the vertical diffusivity (Marotzke, 1991) is increased to $10 \text{ m}^2 \text{ s}^{-1}$. The parameterisation of dense water flow down topographic features of Campin and Goosse (1999) is applied in the model. The experimental set up for the OGCM circulation corresponds to the control run described in Campin et al. (1999). This OGCM was assessed against the global distributions of temperatures, salinities as well as the estimated values of water transport in different locations (North Atlantic, Drake passage, etc.). The circulation of this OGCM reasonably reproduces the pre-bomb $\Delta^{14}\text{C}$ distribution in the deep ocean (Mouchet and Deleersnijder, 2008).
- **LSG-OM** (Maier-Reimer et al., 1993; Mikolajewicz et al., 1993): The Hamburg LSG has been used in a number of climate and ocean tracer studies (e.g. Mikolajewicz et al., 1997; Winguth et al., 1999; Heinze et al., 2003; Dutay et al., 2004). It is based on the conservation laws for heat, salt and momentum, the full equations of state, the hydrostatic approximation and the Boussinesq approximation. The circulation is divided into a barotropic and a baroclinic components, allowing for free surface elevation changes. It also includes a simple sea ice model to account for brine release during freezing. The formulation of the model is fully implicit. It has a horizontal resolution of $3.5^\circ \times 3.5^\circ$ on a E-grid (Arakawa and Lamb, 1977). The water column is subdivided into 11 layers. This model has a smoothed realistic topography. Advection of tracers is solved with the help of an upstream scheme both horizontally and vertically. A horizontal diffusion term ($200 \text{ m}^2 \text{ s}^{-1}$) suppresses mode divergence resulting from the use of a staggered E-grid.

Our offline transport model formulation is very close to that of Heinze et al. (2003). The only difference lies in the treatment of open-ocean convection process, which in our model version takes the form of an explicit diffusion term. As in Heinze and Dittert (2005), the annually averaged fields needed to drive the model represent the pre-industrial ocean state and are obtained from a LSG run resolving the seasonal cycle (Winguth et al., 1999).

10. Appendix C: impact of numerical diffusivity on the leaky funnel parameters

The leaky funnel parameters are determined with the help of M experiments, in which the velocity and explicit diffusivity are homogeneously multiplied by constant factors. Since numerical diffusion is proportional to the velocity magnitude (Roache, 1972), numerical diffusivity in these experiments is affected by the same factor as the velocity field. Hence, the velocity and diffusivity corresponding to experiments i ($i = 1, \dots, M$) may be expressed relatively to those of the unperturbed state as

$$U_i = \gamma_i U \quad \text{and} \quad K_i = \beta_i K^E + \gamma_i K^N, \quad (C1)$$

where β_i and γ_i are constant and positive numbers.

If the leaky funnel adequately represents the circulation in the ocean interior, then the predicted global water age for experiment i , $\langle \hat{a} \rangle_i$, would be given by eq. (21) rewritten with the help of eqs. (26) and (C1):

$$\langle \hat{a} \rangle_i = \frac{L}{U_i} \frac{Pe_i}{1 + Pe_i} = \frac{A_0}{\gamma_i} \frac{1}{1 + \frac{\beta_i}{\gamma_i} \frac{1}{Pe^E} + \frac{1}{Pe^N}}. \quad (C2)$$

Let us consider two working hypotheses: either numerical diffusion is significant or it may be neglected.

Under the first hypothesis (i.e. the standard case), the theoretical model to be fitted to the M 3-D domain averaged ages $\langle a \rangle_i$ is $\langle a \rangle_i(\gamma_i, \beta_i, A_0, Pe^E, Pe^N)$, where $\{A_0, Pe^E, Pe^N\}$ are the three unknown parameters. The best-fit parameters will be those minimising in a least squares sense $\varepsilon(A_0, Pe^E, Pe^N)$ defined as

$$\varepsilon(A_0, Pe^E, Pe^N) = \sum_{i=1}^M \left(\frac{\langle a \rangle_i - \langle \hat{a} \rangle_i(\gamma_i, \beta_i, A_0, Pe^E, Pe^N)}{\sigma_i} \right)^2, \quad (C3)$$

in which σ_i is the standard deviation of the uncertainty associated to $\langle a \rangle_i$. The $\langle \hat{a} \rangle_i$ intervening in eq. (C3) is given by

$$\gamma_i \langle \hat{a} \rangle_i = \frac{A_0}{\left(\frac{Pe^N + 1}{Pe^N} \right)} \frac{\gamma_i / \beta_i}{\left(\frac{Pe^N}{Pe^N + 1} \right) \frac{1}{Pe^E} + \gamma_i / \beta_i}, \quad (C4)$$

which is obtained after some manipulation of eq. (C2). If numerical diffusion is considered to be negligible, then the theoretical model to be fitted is $\langle \hat{a} \rangle_i(\gamma_i, \beta_i, A'_0, Pe'^E)$ with only two unknown parameters $\{A'_0, Pe'^E\}$. We use primed quantities in order to differentiate them from those corresponding to the first case. The cost-function to be minimised in a least squares sense hence reads

$$\varepsilon(A'_0, Pe'^E) = \sum_{i=1}^M \left(\frac{\langle a \rangle_i - \langle \hat{a} \rangle_i(\gamma_i, \beta_i, A'_0, Pe'^E)}{\sigma_i} \right)^2, \quad (C5)$$

in which $\langle \hat{a} \rangle_i$ obeys

$$\gamma_i \langle \hat{a} \rangle_i = A'_0 \frac{\gamma_i / \beta_i}{\frac{1}{Pe'^E} + \gamma_i / \beta_i}. \quad (C6)$$

Expressions (C4) and (C6) correspond to two different theoretical models. Since the γ_i s and β_i s are identical in both cases as are the 3-D domain-averaged water ages $\langle a \rangle_i$, it can readily be seen that replacing A'_0 and Pe'^E in eq. (C6) with the following expressions

$$A'_0 = \left(\frac{Pe^N}{Pe^N + 1} \right) A_0, \quad (C7)$$

$$Pe'^E = \left(\frac{Pe^N + 1}{Pe^N} \right) Pe^E, \quad (C8)$$

results in eq. (C4).

The equalities (C7) and (C8) do not imply that any Pe^N value in eq. (C4) would give equally good fit to the domain-averaged water ages $\langle a \rangle_i$. It is indeed important to note that taking into account numerical diffusion results in an additional constraint on the evolution of $\langle a \rangle_i$ with γ_i .

The respective sets of unknown parameters ($\{A_0, Pe^E, Pe^N\}$ in the first case, $\{A'_0, Pe'^E\}$ in the second case) are obtained from the minimisation of the cost function for two different problems. Hence, they represent the best-fit set of parameters that may be obtained in each case. When neglecting numerical diffusion the apparent A_0 decreases while the apparent Pe increases as predicted by eqs. (C7) and (C8) such that

$$\langle \hat{a} \rangle_i = \langle \hat{a}' \rangle_i. \quad (C9)$$

We obtained the parameter sets corresponding to the two problems (C3) and (C5) for each OGCM. The results are given in Table 3. It is readily seen from the table that the values $\{A_0, Pe^E, Pe^N\}$ and $\{A'_0, Pe'^E\}$ obtained with both OGCMs satisfy the ratios (C7) and (C8).

Since eq. (C9) holds true, there is no impact on the fit of water age. Predicted water ages are exactly the same under both hypotheses (Table 3). This agreement occurs because any decrease in A_0 is balanced by the increase of Pe . The correlation coefficient as well as the mean residual in the

case of water age are strictly identical whether or not numerical diffusion is considered. The constraint (C9) is also valid for the global water age distribution since it is implicit from the mathematical development in Section 2 that $\phi(\tau)$ must verify $\int_0^\infty \tau \phi(\tau) d\tau = \langle a \rangle$.

The situation is different for the ages of radioactive tracers whose analytical expression involves cross products of α_i and β_i . The linear correlation coefficient increases and the mean residual decreases when the estimate of the leaky funnel parameter is performed while including numerical diffusion. Hence, for radioactive tracer ages, eq. (C4) leads to better result than eq. (C6) (Mouchet, 2011).

11. Appendix D: erratum for MD08

It appears that typing errors affected several equations in MD08. The correct versions follow:

Equations (9) and (10) of MD08 should read:

$$S \frac{\partial C_\lambda}{\partial t} + \frac{\partial(SUC_\lambda)}{\partial x} = C_\lambda \frac{\partial(US)}{\partial x} + \frac{\partial}{\partial x} \left(SK \frac{\partial C_\lambda}{\partial x} \right) - \lambda SC_\lambda,$$

$$S \frac{\partial \alpha_\lambda}{\partial t} + \frac{\partial(SU\alpha_\lambda)}{\partial x} = \alpha_\lambda \frac{\partial(US)}{\partial x} + \frac{\partial}{\partial x} \left(SK \frac{\partial \alpha_\lambda}{\partial x} \right) - \lambda S\alpha_\lambda + SC_\lambda.$$

The correct expression for the volume distribution of water age (third equation in Appendix A of MD08) is

$$\phi(a_w) = \frac{e^{-a_w/\langle a_w \rangle}}{\langle a_w \rangle}.$$

References

- Abramowitz, M. and Stegun, I. 1972. *Handbook of Mathematical Functions*. 9th edn. Dover Publications, New York, 1030 pp.
- Arakawa, A. and Lamb, V. R. 1977. Computational design of the basic dynamical process of the UCLA general circulation model. *Methods Comput. Phys.* **17**, 173–265.
- Beckers, J.-M., Delhez, E. J. M. and Deleersnijder, E. 2001. Some properties of generalized age-distribution equations in fluid dynamics. *SIAM J. Appl. Math.* **61**, 1526–1544.
- Bolin, B. and Rodhe, H. 1973. A note on the concepts of age distribution and transit time in natural reservoirs. *Tellus* **25**, 58–62.
- Broecker, W. S. and Peng, T.-H. 2000. Comparison of ^{39}Ar and ^{14}C ages for waters in the deep ocean. *Nucl. Instrum. Meth. B* **172**, 473–478.
- Burchard, H. and Rennau, H. 2008. Comparative quantification of physically and numerically induced mixing in ocean models. *Ocean Model.* **20**, 293–311. DOI: 10.1016/j.ocemod.2007.10.003.
- Campin, J.-M., Fichefet, T. and Duplessy, J.-C. 1999. Problems with using radiocarbon to infer ocean ventilation rates for past and present climates. *Earth Planet. Sci. Lett.* **165**, 17–24.
- Campin, J.-M. and Goosse, H. 1999. Parameterization of density-driven downsloping flow for a coarse-resolution ocean model in z-coordinate. *Tellus* **51**, 412–430.
- Craig, H. 1971. The deep metabolism: oxygen consumption in abyssal ocean water. *J. Geophys. Res.* **76**, 5078–5086.
- Deleersnijder, E., Beckers, J.-M., Campin, J.-M., El Mohajir, M., Fichefet, T. and co-authors. 1997. Some mathematical problems associated with the development and use of marine models. In: *The Mathematics of Models for Climatology and Environment, NATO ASI Series* (ed. J. I. Diaz) Vol. I48, Springer Verlag, Berlin/Heidelberg, pp. 39–86.
- Deleersnijder, E. and Campin, J.-M. 1995. On the computation of the barotropic mode of a free-surface world ocean model. *Ann. Geophys.* **13**, 675–688.
- Deleersnijder, E., Campin, J.-M. and Delhez, E. 2001. The concept of age in marine modelling. I. Theory and preliminary model results. *J. Marine Syst.* **28**, 229–267.
- Deleersnijder, E., Mouchet, A., Delhez, E. and Beckers, J.-M. 2002. Transient behaviour of water ages in the world ocean. *Math. Comput. Model.* **36**, 121–127.
- Deleersnijder, E., Wang, J. and Mooers, C. N. K. 1998. A two-compartment model for understanding the simulated three-dimensional circulation in Prince William Sound, Alaska. *Cont. Shelf Res.* **18**, 279–287.
- Delhez, E., Campin, J.-M., Hirst, A. C. and Deleersnijder, E. 1999. Toward a general theory of the age in ocean modelling. *Ocean Model.* **1**, 17–27.
- Delhez, E. and Deleersnijder, E. 2002. The concept of age in marine modelling: II. Concentration distribution function in the English Channel and the North Sea. *J. Marine Syst.* **31**, 279–297.
- Delhez, E., Deleersnijder, E., Mouchet, A. and Beckers, J.-M. 2003. A note on the age of radioactive tracers. *J. Marine Syst.* **38**, 277–286.
- Doney, S. C., Lindsay, K., Caldeira, K., Campin, J.-M., Drange, H. and co-authors. 2004. Evaluating global ocean carbon models: the importance of realistic physics. *Global Biogeochem. Cycles* **18**, GB3017. DOI: 10.1029/2003GB00215.
- Dutay, J.-C., Jean-Baptiste, P., Campin, J.-M., Ishida, A., Maier-Reimer, E. and co-authors. 2004. Evaluation of OCMIP-2 ocean models' deep circulation with mantle helium-3. *J. Marine Syst.* **48**, 15–36. DOI: 10.1016/j.jmarsys.2003.05.010.
- Gradshteyn, I. and Ryzhik, I. 2000. *Tables of Integrals, Series, and Products*. 6th ed. Academic Press, San Diego.
- Haine, T. W. N. and Hall, T. M. 2002. A generalized transport theory: water-mass composition and age. *J. Phys. Oceanogr.* **32**, 1932–1946.
- Hall, T. M. and Haine, T. W. N. 2002. On ocean transport diagnostics: the idealized age tracer and the age spectrum. *J. Phys. Oceanogr.* **32**, 1987–1991. DOI: 10.1175/1520-0485.
- Hall, T. M., Haine, T. W. N., Holzer, M., Lebel, D. A., Terenzi, F. and co-authors. 2007. Ventilation rates estimated from tracers in the presence of mixing. *J. Phys. Oceanogr.* **37**, 2599–2611. DOI: 10.1175/2006JPO3471.1.
- Hall, T. M. and Holzer, M. 2003. Advective-diffusive mass flux and implications for stratosphere-troposphere exchange. *Geophys. Res. Lett.* **30**, 1222. DOI: 10.1029/2002GL016419.

- Heinze, C., Hupe, A., Maier-Reimer, E., Dittert, N. and Ragueneau, O. 2003. Sensitivity of the marine biospheric Si cycle for biogeochemical parameter variations. *Global Biogeochem. Cycles* **17**, 1086.
- Heinze, C. and Dittert, N. 2005. Impact of paleocirculations on the silicon redistribution in the world ocean. *Mar. Geol.* **214**, 201–213.
- Heinze, C., Maier-Reimer, E. and Winn, K. 1991. Glacial pCO₂ reduction by the world ocean: experiments with the Hamburg carbon cycle model. *Palaeoceanography* **6**, 395–430.
- Holzer, M. and Primeau, F. W. 2006. The diffusive ocean conveyor. *Geophys. Res. Lett.* **33**, L14,618. DOI: 10.1029/2006GL026232.
- Huang, R. X. 1999. Mixing and energetics of the oceanic thermohaline circulation. *J. Phys. Oceanogr.* **29**, 727–746.
- Jenkins, W. J. 1998. Studying subtropical thermocline ventilation and circulation using tritium and ³He. *J. Geophys. Res.* **103**, 15817–15831.
- Kuhlbrodt, T., Griesel, A., Montoya, M., Levermann, A., Hofmann, M. and co-authors. 2007. On the driving processes of the Atlantic meridional overturning circulation. *Rev. Geophys.* **45**, RG2001. DOI: 10.1029/2004RG000166.
- Kunze, E., Firing, E., Hummon, J. M., Chereskin, T. K. and Thurnherr, A. M. 2006. Global abyssal mixing inferred from lowered ADCP shear and CTD strain profiles. *J. Phys. Oceanogr.* **36**, 1553–1576 (Corrigendum, pp. 2350–2352).
- Ledwell, J. R., Watson, A. J. and Law, C. S. 1993. Evidence for slow mixing across the pycnocline from an open-ocean tracer-release experiment. *Nature* **364**, 701–703. DOI: 10.1038/364701a0.
- Maier-Reimer, E. 1993. Geochemical cycles in an ocean general circulation model. Preindustrial tracer distributions. *Global Biogeochem. Cycles* **7**, 645–677.
- Maier-Reimer, E., Mikolajewicz, U. and Hasselmann, K. 1993. Mean circulation of the Hamburg LSG OGCM and its sensitivity to the thermohaline surface forcing. *J. Phys. Oceanogr.* **23**, 731–757.
- Markwardt, C. B. 2009. Non-linear least-squares fitting in IDL with MPFIT. *Astr. Soc. P.* **411**, 251–254. Online at: <http://purl.com/net/mpfit>.
- Marotzke, J. 1991. Influence of convective adjustment on the stability of the thermohaline circulation. *J. Phys. Oceanogr.* **21**, 903–907.
- Mikolajewicz, U., Crowley, T. J., Schiller, A. and Voss, R. 1997. Modeling North Atlantic/North Pacific teleconnections during the Younger Dryas. *Nature* **387**, 384–387.
- Mikolajewicz, U., Maier-Reimer, E., Crowley, T. J. and Kim, K. 1993. Effect of Drake and Panamanian Gateways on the circulation of an ocean model. *Palaeoceanography* **8**, 4. DOI: 10.1029/93PA00893.
- Moré, J. 1978. The Levenberg-Marquardt algorithm: implementation and theory. *Numer. Anal.* **630**, 105. DOI: 10.1007/BFb006769.
- Mouchet, A. 2011. *A 3D Model of Ocean Biogeochemical Cycles and Climate Sensitivity Studies*. Ph.D. Thesis, Université de Liège, Liège, Belgium.
- Mouchet, A. and Deleersnijder, E. 2008. The leaky funnel model, a metaphor of the ventilation of the World Ocean as simulated in an OGCM. *Tellus* **60A**, 761–774. DOI: 10.1111/j.1600-0870.2008.00322.x.
- Munk, W. 1966. Abyssal recipes. *Deep-Sea Res.* **13**, 707–730.
- Munk, W. and Wunsch, C. 1998. Abyssal recipes II: energetics of tidal and wind mixing. *Deep-Sea Res.* **45**, 1977–2010.
- Olbers, D. and Wenzel, M. 1989. Determining diffusivities from hydrographic data by inverse methods with application to the circumpolar current. In: *Oceanic Circulation Models: Combining Data and Dynamics* (eds. D. L. T. Anderson and J. Willebrand), Kluwer Academic Publishers, Dordrecht, pp. 95–139.
- Oschlies, A. 2000. Equatorial nutrient trapping in biogeochemical ocean models: the role of advection numerics. *Global Biogeochem. Cycles* **14**, 655–667.
- Pacanowski, R. C. and Philander, S. G. H. 1981. Parameterization of vertical mixing in numerical models of tropical oceans. *J. Phys. Oceanogr.* **11**, 1443–1451.
- Peacock, S. and Maltrud, M. 2006. Transit-time distributions in a global ocean model. *J. Phys. Oceanogr.* **36**, 474–495. DOI: 10.1175/JPO2860.1.
- Polzin, K. L., Toole, J. M., Ledwell, J. R. and Schmitt, R. W. 1997. Spatial variability of turbulent mixing in the Abyssal Ocean. *Science* **276**, 93–96.
- Primeau, F. and Deleersnijder, E. 2009. On the time to tracer equilibrium in the global ocean. *Ocean Sci.* **5**, 13–28. Online at: www.ocean-sci.net/5/13/2009/.
- Primeau, F. W. and Holzer, M. 2006. The oceans memory of the atmosphere: residence-time and ventilation-rate distributions of water masses. *J. Phys. Oceanogr.* **36**, 1439–1456. DOI: 10.1175/JPO2919.1.
- Roache, P. 1972. On artificial viscosity. *J. Comput. Phys.* **10**, 169–184.
- Saenko, O. A., Zhai, X., Merryfield, W. J. and Lee, W. G. 2012. The combined effect of tidally and eddy-driven diapycnal mixing on the large-scale ocean circulation. *J. Phys. Oceanogr.* **42**, 526–538. DOI: 10.1175/JPO-D-11-0122.1.
- Schmittner, A., Urban, N. M., Keller, K. and Matthews, D. 2009. Using tracer observations to reduce the uncertainty of ocean diapycnal mixing and climate carbon cycle projections. *Global Biogeochem. Cycles* **23**, GB4009. DOI: 10.1029/2008GB003421.
- Schmittner, A. and Weaver, A. 2001. Dependence of multiple climate states on ocean mixing parameters. *Geophys. Res. Lett.* **28**, 1027–1030.
- St Laurent, L. and Simmons, H. 2006. Estimates of power consumed by mixing in the ocean interior. *J. Clim.* **19**, 4877–4890.
- Stommel, H. and Arons, A. 1960a. On the abyssal circulation of the world ocean – I. Stationary planetary flow patterns on a sphere. *Deep-Sea Res.* **6**, 140–154.
- Stommel, H. and Arons, A. 1960b. On the abyssal circulation of the world ocean – II. An idealized model of the circulation pattern and amplitude in ocean basins. *Deep-Sea Res.* **6**, 217–233.
- Stuiver, M., Östlund, H. and McConnaughey, T. 1981. GEOSECS Atlantic and Pacific ¹⁴C distribution. In: *Carbon Cycle*

- Modelling* (ed. B. Bolin). John Wiley & Sons, New York, pp. 201–221.
- Tartinville, B., Deleersnijder, E. and Rancher, J. 1997. The water residence time in the Mururoa atoll lagoon: a three-dimensional model sensitivity analysis. *Coral Reefs* **6**, 193–203.
- Toggweiler, J. R., Dixon, K. and Bryan, K. 1989. Simulations of radiocarbon in a coarse-resolution world ocean model. 1. Steady state prebomb distributions. *J. Geophys. Res.* **94**, 8217–8242. DOI: 10.1029/JC094iC06p08217.
- Toole, J. and McDougall, T. 2001. Mixing and stirring in the ocean interior. In: *Ocean Circulation and Climate* (eds. G. Siedler, J. Church and J. Gould) Chap. 5.2, Academic Press, San Diego, USA, pp. 337–356.
- Webb, D. J. and Sugimotohara, N. 2001. The interior circulation of the ocean. In: *Ocean Circulation and Climate* (eds. G. Siedler, J. Church and J. Gould) Chap. 4.2, Academic Press, San Diego, USA, pp. 205–213.
- Winguth, A. M. E., Archer, D., Duplessy, J.-C., Maier-Reimer, E. and Mikolajewicz, U. 1999. Sensitivity of paleonutrient tracer distributions and deep-sea circulation to glacial boundary conditions. *Palaeoceanography* **14**, 304–323.
- Zhang, J., Schmitt, R. W. and Huang, R. X. 1999. The relative influence of diapycnal mixing and hydrologic forcing on the stability of the thermohaline circulation. *J. Phys. Oceanogr.* **29**, 1096–1108.